NANO LETTERS
Letter
Cite This: Nano Lett. 2018, 18, 5078−5084
pubs.acs.org/NanoLett

Enhanced Light Emission from the Ridge of Two-Dimensional InSe Flakes

Yang Li,[†,▽,○] Tianmeng Wang,[†,○] Han Wang,[‡,○] Zhipeng Li,[†,∥] Yanwen Chen,[†] Damien West,[‡] Raman Sankar,[⊥,#] Rajesh K. Ulaganathan,[⊥,#] Fangcheng Chou,[⊥,#] Christian Wetzel,[‡] Cheng-Yan Xu,[*,▽] Shengbai Zhang,[*,‡] and Su-Fei Shi[*,†,§]

[†]Department of Chemical and Biological Engineering, [‡]Department of Physics and Astronomy, and [§]Department of Electrical, Computer and Systems Engineering, Rensselaer Polytechnic Institute, Troy, New York 12180, United States
[∥]School of Chemistry and Chemical Engineering, Shanghai Jiao Tong University, Shanghai 200240, China
[⊥]Institute of Physics, Academia Sinica, Nangang, Taipei, Taiwan 11529, Taiwan
[#]Center for Condensed Matter Science, National Taiwan University, Taipei, Taiwan 10617, Taiwan
[▽]School of Materials Science and Engineering, Harbin Institute of Technology, Harbin 150001, China

Supporting Information

ABSTRACT: InSe, a newly rediscovered two-dimensional (2D) semiconductor, possesses superior electrical and optical properties as a direct-band-gap semiconductor with high mobility from bulk to atomically thin layers and is drastically different from transition-metal dichalcogenides, in which the direct band gap only exists at the single-layer limit. However, absorption in InSe is mostly dominated by an out-of-plane dipole contribution, which results in the limited absorption of normally incident light that can only excite the in-plane dipole at resonance. To address this challenge, we have explored a unique geometric ridge state of the 2D flake without compromising the sample quality. We observed the enhanced absorption at the ridge over a broad range of excitation frequencies from photocurrent and photoluminescence (PL) measurements. In addition, we have discovered new PL peaks at low temperatures due to defect states on the ridge, which can be as much as ∼60 times stronger than the intrinsic PL peak of InSe. Interestingly, the PL of the defects is highly tunable through an external electrical field, which can be attributed to the Stark effect of the localized defects. InSe ridges thus provide new avenues for manipulating light−matter interactions and defect engineering that are vitally crucial for novel optoelectronic devices based on 2D semiconductors.

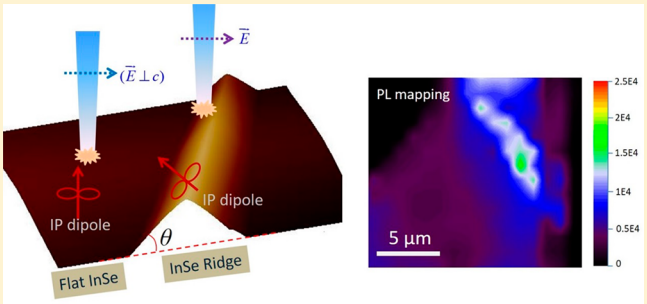

KEYWORDS: *Indium selenide, ridges, selection rules, defect emission, stark effect*

Two-dimensional (2D) semiconductors have attracted intense research interest because of their well-defined band gap and atomic-scale thickness, promising optoelectronics applications beyond the scaling limit.[1−3] As the most-studied 2D semiconductors, transition-metal dichalcogenides (TMDCs) undergo an indirect to direct band-gap transition when they are thinned to the monolayer limit.[4,5] Furthermore, monolayer TMDCs (such as MoS_2, WSe_2, etc.) exhibit rich exciton physics and possess an additional valley degree of freedom.[6−8] However, the relatively low carrier mobility and low absorption associated with a monolayer impede the development of electronic and optoelectronic application based on TMDCs.[9−12]

In contrast, bulk InSe has a direct band gap at the Z point of the Brillouin zone,[13−16] and its mobility can be as high as ∼20 000 $cm^2/(V\ s)$.[14] Interestingly, InSe retains both the direct band gap feature and high carrier mobility down to a few atomic layers, rendering it a promising candidate for nanoscale high-speed optoelectronic applications.[17−20] However, the orbital character of the band edges are distinct from TMDCs, leading to altered optical selection rules. In particular, the conduction band minimum (CBM) of InSe is dominated by the s orbital of the In atom, and the first valence band maximum, VBM is dominated by the p_z oribtal of the Se atom (Figure 1b).[15,21] As a result, the absorption dipole is out-of-plane and cannot be directly excited by a normally incident light at resonance, as prohibited by the selection rule ($\boldsymbol{E} \perp \boldsymbol{c}$ is forbidden, as shown in Figure 1b).[22−25] This forbidden transition for normally incident excitation, only allowed by mixing with the deeper valence bands with Se p_{xy} character or by excitation with excess photon energy, hinders potential optoelectronic applications based on InSe, in which a response to normally incident light is often required. Previously, InSe

Received: May 12, 2018
Revised: June 21, 2018
Published: July 19, 2018

DOI: 10.1021/acs.nanolett.8b01940
Nano Lett. 2018, 18, 5078−5084

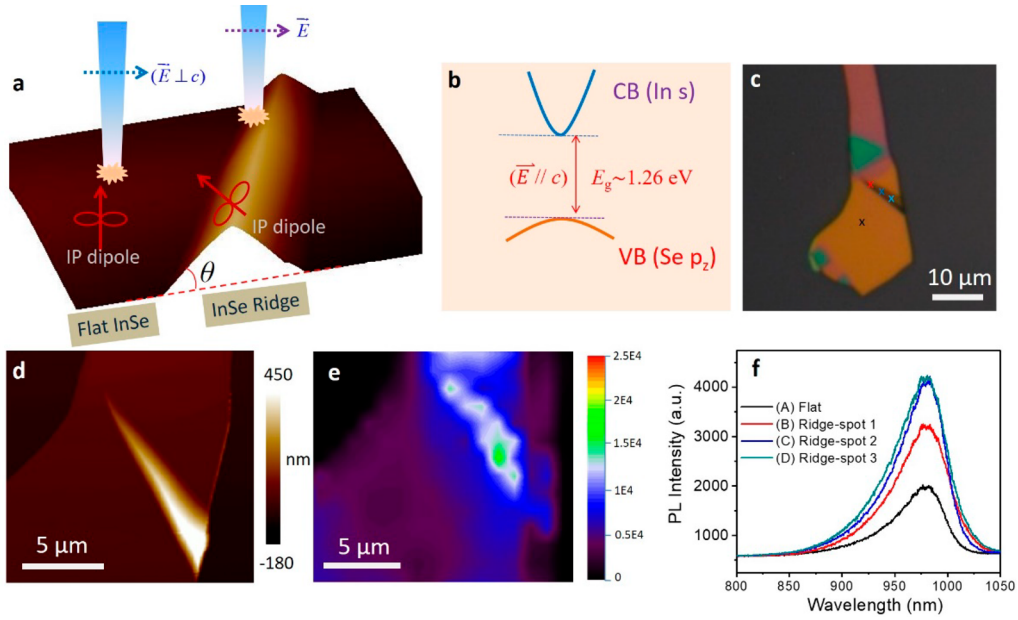

Figure 1. PL enhancement from the ridge of a 2D InSe flake. (a) A schematic of the in-plane (IP) emission dipole orientation with the normally incident light exciting both the flat and ridge region of the InSe flake. θ denotes the angle of the ridge. (b) A schematic of the bandstructure of bulk InSe at the Z point. The first interband transition is dominantly induced by the optical field parallel to the c axis of InSe. (c) Optical microscope image and (d) AFM topography of an InSe flake with a ridge. (e) The spatially resolved PL mapping of the InSe flake containing the ridge shown in (d). (f) The PL spectra from the positions in panel c show enhanced PL at the ridge compared to that from the flat region.

flakes were coupled to a silica-nanoparticle-roughened substrate to increase the coupling to the normally incident light, resulting in the enhancement of both light absorption and light emission.[24]

In this work, we exploit a unique topology feature, naturally formed ridges in a 2D InSe flake, to address this challenge by coupling the electrical field of the incident light with the out-of-plane dipole moment. The InSe ridge in a 2D flake, schematically shown in Figure 1a,b, allows the optical field of the normally incident light to couple with the originally in-plane dipole. We employed photoluminescence (PL) spectroscopy and scanning photocurrent microscopy (SPCM) to reveal the emission and absorption enhancement. In addition, we observed new PL peaks at low temperatures due to defect states at the ridge, which can be ~60 times stronger than the intrinsic PL of InSe. Interestingly, the PL of the defects is highly tunable by a gate voltage through the Stark effect, which is attributed to the localized nature of the defects.

InSe was mechanically exfoliated on a Si/SiO_2 substrate with an oxide layer of 300 nm, and large flakes with ridges (Figure 1c) were often found. From the atomic force microscopy (AFM) topography, we determined the thickness of the flake in Figure 1d to be approximately 80 nm, and the height and width of the ridge are about 350 nm and 2 μm, respectively. This corresponds to a θ (Figure 1a) of 19.3°. We have measured more than 20 ridges and found that the average angle (θ) of the ridge varies from 10° to 30° (see Figure S1). We further carried out the spatially resolved PL mapping of the flake at room temperature. As shown in Figure 1e, the PL from the flat region is relatively homogeneous, while that from the ridge region shows inhomogeneity and is evidently enhanced. Detailed PL spectra from different spots on the ridge is shown in Figure 1f, in which PL from the ridge is enhanced by ~2.6 times compared to that from the flat region (black curve in Figure 1f). We note, however, that the PL spectra from both the ridge region and the flat region are centered at ~985 nm (~1.26 eV). This corresponds to the transition from the first VBM to CBM at the Z point, as shown in Figure 1b, and is consistent with previous reports of 2D InSe.[15,17,24] Similar PL enhancement has been observed in more than 20 InSe ridges that we have investigated, with the thickness varying from ~25 to ~120 nm (part II in the Supporting Information).

We performed photocurrent measurements of the devices based on the InSe ridge, with the consideration that the photocurrent is proportional to the absorption of the semiconductor.[26−28] The device was fabricated by evaporating gold electrodes using a shadow mask to a preidentified few-layer InSe flake with a ridge, avoiding possible deformation or contamination of the ridge induced by photolithography or e-beam lithography. A typical device is shown in Figure 2a, and the few-layer InSe flake is about 60 nm thick. The electrical transport property was characterized with current−voltage (I−V) measurements at 77 K (Figure 2b) with and without light illumination on the ridge. The device shows a low dark current but a large photocurrent response to the light and an on-to-off ratio exceeding 1000 at the bias voltages of 200 and −200 mV. This sensitive response to light can be exploited for applications in photodetectors.

The spatially resolved photocurrent was obtained by scanning photocurrent microscopy (SPCM) measurements to distinguish the different response from the flat and ridge region of the InSe flake at 77 K with a CW laser excitation centered at 532 nm. Figure 2c shows the spatially resolved photocurrent response at a bias voltage of 100 mV near the right electrical contact. The photocurrent near the left electrical contact at 100 mV and photocurrent mapping at −100 mV are shown in part III of the Supporting Information. By comparing the SPCM maps with the reflection images obtained simultaneously (see Figures S7 and S8), it is evident that the photocurrent response is dominated by the

DOI: 10.1021/acs.nanolett.8b01940
Nano Lett. 2018, 18, 5078−5084

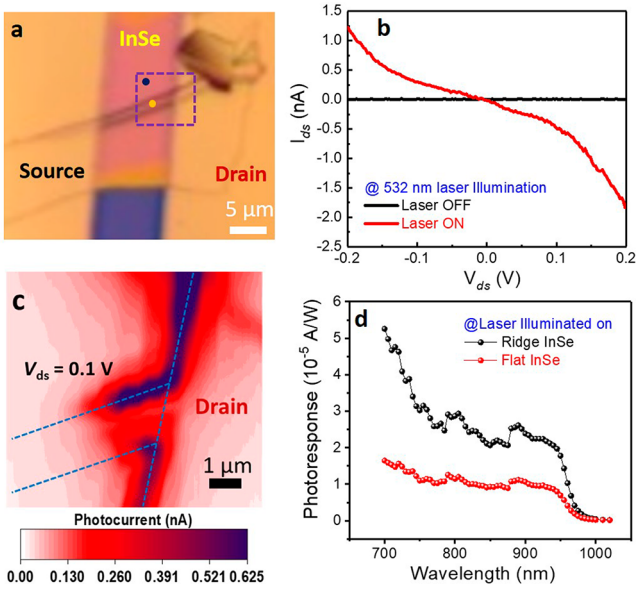

Figure 2. Photocurrent enhancement from the InSe ridge. (a) Optical image of a multilayer InSe device for photocurrent measurements. The thickness of the flake is about 60 nm. (b) $I-V$ curves of the InSe device with or without CW laser (λ = 532 nm) illuminating on the ridge. The yellow (black) circle in Figure 2a is the laser illumination spot on the InSe ridge (flat InSe), and the excitation power is 10 μW. (c) Spatially resolved photocurrent image of the device with the source-drain voltage of 100 mV and the excitation power of 10 μW. The blue dashed lines outline the edges of the ridge, and the yellow dashed line is the contact interface between Au and InSe. The scanning area is shown as the square in panel a. (d) Photocurrent at the bias voltage of 100 mV as a function of excitation wavelength on the flat and ridge region of the InSe flake.

contribution from the contact and along the ridge area. The enhanced photocurrent from the Au−InSe interface can be attributed to the enhanced driving force, originating from the built-in field at the junction. The enhancement from the ridge, however, is of a different nature. With the absence of the built-in field, the enhancement of photocurrent is due to the enhancement of photoconductivity, which originates from the absorption enhancement. This interpretation is confirmed in Figures S7 and S8, in which the photocurrent from the ridge (and the flat region) changes sign as the bias voltage switches from positive to negative. To further investigate the nature of the enhanced photoconductivity at the ridge, we measured the photoconductivity enhancement as a function of the excitation light wavelength. As shown in Figure 2d, the photocurrent from both the flat and the ridge region of the InSe flake exhibit similar band-edge rising behavior as the exciting wavelength is shorter than ~975 nm, consistent with our observation of the PL spectra in Figure 1f. Once above the band edge, the photocurrent on the ridge is enhanced over a broad range of excitation wavelength (700 to ~950 nm) by a factor of 2−3.

Both the PL enhancement and photoconductivity enhancement of the InSe ridge can be explained with the absorption enhancement. Per our previous discussion of the out-of-plane dipole, the enhancement of absorption (η) on the ridge originates from the increased out-of-plane component of the optical field, and it can be expressed as:

$$\eta = \alpha_{E_\perp}\cos\theta + \alpha_{E_\parallel}\mathrm{Sin}\theta \quad (1)$$

where η, $\alpha_{E_\perp}$,$\alpha_{E_\parallel}$, and θ are effective absorption on the ridge, absorption coefficient for $E\perp c$, absorption coefficient for $E//c$, and incident angle determined by AFM measurement of the ridge. Previous first-principles calculations have reported the ratio of $\alpha_{E_\perp}$ to $\alpha_{E_\parallel}$ at an excitation wavelength of 532 nm to be ~6.[24] Considering that the incident angle θ in Figure 2a is ~22°, the predicted absorption anisotropy of 6 will lead to enhanced power absorption of 3.2, which is in good agreement with our observation of the enhanced PL and photoconductivity. Additional PL enhancement from improved coupling of the emission dipole to free space was not observed. This lack of additional enhancement is partly due to the excessive energy of the excitation photon, which allows for phonon-assisted recombination, relaxing the restriction of the selection rule and partly due to the large NA of the objective (~0.6), which collects emitted photons with a large solid angle.

Interestingly, new PL peaks emerge on InSe ridge at low temperatures. As shown in Figure 3a, a new PL peak (labeled as D) centered at ~995 nm emerges on the InSe ridge at 77 K, along with the intrinsic exciton PL peak (A) centered at ~960 nm, which is the same as the PL from the flat InSe (black curve in Figure 3a). The excitation power dependence of the new PL peak (D) is different from the intrinsic PL of flat InSe (A). We plot the integrated PL signal from the ridge as a function of the excitation power in Figures 3b and S10. PL intensity from the A and D peaks depend on power nonlinearly as ~P^α, where P is the excitation power. The fitting of the experimental data shows that α is ~1.5 for the A peak and ~1.2 for the D peak. The obtained superlinear power dependence of the A peak with the exponent of ~1.5 suggests that the PL of peak A at 77 K has a dual nature of free carrier and excitonic behavior due to the small exciton binding energy. The power exponent of peak D clearly differs from that of the peak A and is closer to 1.

Cooling the InSe sample to a lower temperature introduces even-more-striking changes to the PL spectra from the InSe ridge. Figure 3c shows the PL spectra of flat InSe and InSe ridge at 7 K. It is observed that not only does the new PL peak (D) split into two peaks (D_1 and D_2), but also, the PL intensities of the D_1 and D_2 peaks are drastically enhanced compared to that of A peak from the ridge, with the enhancement factor of ~60 for D_1 and ~20 for D_2. The PL intensities from the defects are also greatly enhanced compared to that from the flat region (black curve in Figure 3c). Detailed temperature evolution of the PL from flat InSe and the InSe ridge are shown as normalized PL in Figure 3d,e. PL from the flat InSe flake (Figure 3d) shows a blue shift of the exciton peak A as the temperature is decreased, which can be described by the empirical Varshni relation as in traditional semiconductors.[29]

The integrated intensities of A, D_1, and D_2 peaks as a function of temperature are shown in Figure 3f. The nearly 2 orders of magnitude increase of PL intensity of the D_1 peak versus the A peak is evident at 7 K. The intensity of all three peaks are associated with an activation behavior as the temperature changes and can be fitted by an Arrhenius eq (as shown in Figure 3f): $I(T) = \frac{I_0}{1 + A\exp(-E_B / k_B T)}$, where I_0, E_B, and k_B are the PL intensity at 0 K, the thermal activation energy, and the Boltzmann constant, respectively. The binding energy of A peak is estimated to be 16.4 meV, which is close to the previously reported value of exciton binding energy in bulk InSe (14.5 meV).[30−33] Arrhenius fitting of the peak D_1 and D_2

DOI: 10.1021/acs.nanolett.8b01940
Nano Lett. 2018, 18, 5078−5084

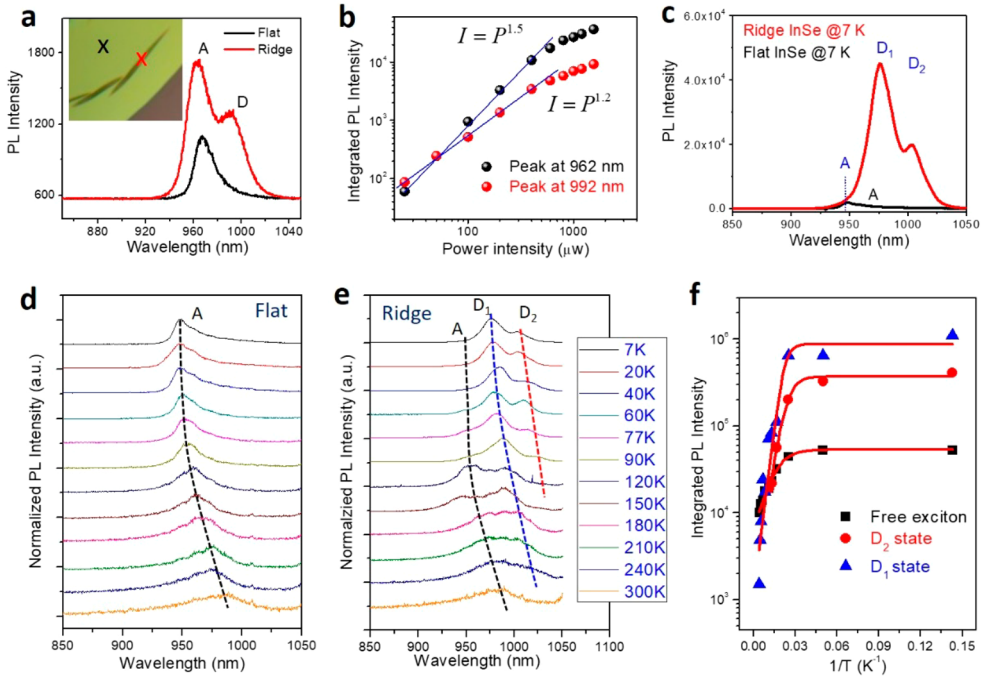

Figure 3. Enhanced PL from defects on the InSe ridge. (a) PL spectra of the flat (dark ×) and ridge (red ×) region of a InSe flake at 77 K. Inset: optical image of the InSe flake with ridges. (b) Integrated PL intensity as a function of the excitation power for the two peaks at 960 and 995 nm at 77 K. (c) PL spectra of the flat InSe and InSe ridge at 7 K. (d, e) Temperature-dependent PL spectra of the flat InSe and InSe ridge from 7 to 300 K, respectively. "A" represents the photon emission from the free exciton, while "D_1" and "D_2" are from emission due to the newly formed defects. PL spectra in panels c and d are renormalized for comparison. (f) The integrated PL intensity of the A, D_1, and D_2 peaks as a function of reciprocal temperature from 7 to 300 K. The integrated PL intensity of the A exciton dependence on the temperature is extracted from the flat InSe, where those of D_1 and D_2 are extracted from ridge InSe.

results in the defect binding energy of 35.3 meV (D_1) and 25.6 meV (D_2), respectively. The larger binding energy from the defects results in the red shift of the D_1 and D_2 peak compared to that of the A peak. The small binding energy of the A peak indicates that the band edge transition dominates the PL at room temperature.

The activation behavior of the PL suggests that the new peaks are from defects. But why would defects form at the ridge? A close examination of the AFM topography of the InSe ridge (Figure 1d) suggests that the geometry will induce a strain as high as ∼8.8% in the InSe flake if there is no mechanical breakdown.[34,35] This large strain could mechanically break bonds locally at the ridge, which releases the strain and introduces defect states. This is supported by our separate study of strain effect on InSe flake, which revealed an extremely sensitive strain-induced band gap change rate (∼150 meV/% strain), without the appearance of additional PL peaks.[36] This hypothesis is also supported by our control experiments in which we intentionally introduce strain into InSe by forming wrinkles in an InSe flake, which is fabricated through exfoliation on a strained PDMS film, followed by releasing the strain in PDMS (see the Supporting Information). PL from the InSe winkles show a significant peak shift even at room temperature. PL from the InSe ridge at low temperatures, however, exhibits the intrinsic A peak at the same wavelength (emission photon energy) as the PL from the flat InSe, indicating the absence of strain in the ridge. The additional peaks thus can be attributed to the newly formed defects, with the activation energies given by the previous fitting with the Arrhenius equation.

The localized nature of the defect would suggest a sensitive dependence on the electrical field through the Stark effect.[37−39] We thus fabricated InSe devices and used a back-gate voltage to apply an out-of-plane electrical field to investigate the PL change from the InSe ridge. For a typical device as shown in Figure 4a, the PL spectrum from the ridge at 77 K with no gate voltage applied is shown in Figure 4b, in which both the intrinsic exciton and the defect emission are observed. The gate-voltage-dependent PL spectra from the InSe ridge is shown in a color plot in Figures 4c and S7). As shown in Figure 4c, in addition to the enhanced PL amplitude, the new PL peak exhibits two features that are qualitatively distinct from the intrinsic exciton peak. (1) The intensity of intrinsic exciton peak quenches from gate voltage of −40 to ∼0 V, while the maximum intensity of the new PL peak is located at gate voltage ∼0 V and remains strong from −50 to 30 V. (2) The intrinsic exciton peak position remains roughly at the same wavelength, while the new PL peak position sensitively depends on the gate voltage applied.

Both features can be explained with the interpretation that the new PL peak originates from localized defects. First, the quenching of the exciton PL has been widely observed in gated monolayer TMDCs devices, in which the addition of free carrier significantly enhances the nonradiative channels.[43,44] Localized defects, however, are less sensitive to the presence of free carriers. Second, it has been shown in previous reports that the Stark effect is enhanced in quantum confined systems.[37,38,40] As suggested by the previously extracted activation energies, the defects are much more localized than the exciton, and hence, the PL is more sensitive to the electrical field.

DOI: 10.1021/acs.nanolett.8b01940
Nano Lett. 2018, 18, 5078−5084

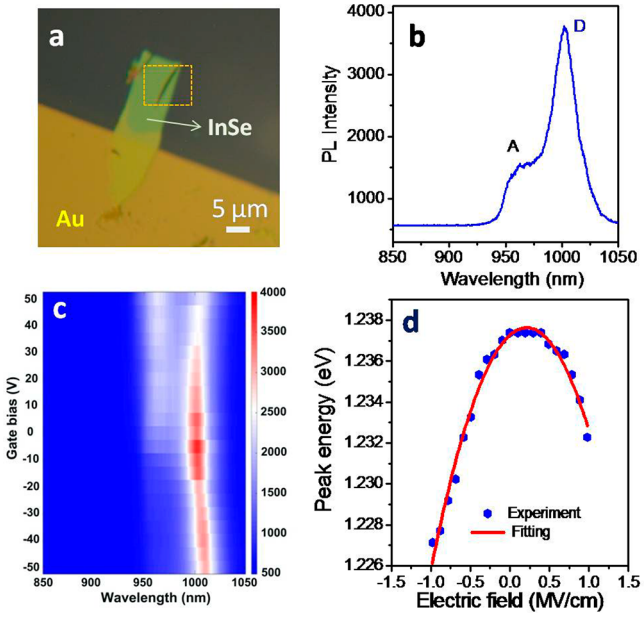

Figure 4. Gate voltage tunable PL spectra. (a) Optical image of the InSe device on which we performed the PL measurements at different gate voltages. (b) Typical PL spectra from the InSe ridge at 77 K. (c) PL intensity of the InSe ridge as a function of the emission wavelength and gate voltage at 77 K. (d) The new PL peak position (emission photon energy) from the InSe ridge as a function of the electric field at 77 K.

We can quantitatively understand the defect dipole moment by investigating the PL shift as a function of the gate-voltage dependence (Figure 4c). To achieve this, we convert the gate voltage to the electrical field using the 300 nm thickness of the oxide layer with a simple capacitor model. Due to the complicated geometry of ridge, the extracted electrical field will be an estimate of the upper bound. The detailed emission photon energy from defects as a function of the external electrical field is plotted in Figure 4d. The dependence of the defect PL peak on the electric field can be fitted with a quadratic function:[39,40]

$$E(F) = E_0 - pF - \beta F^2 \quad (2)$$

where E_0, p, F, and β are the defect emission energy without the electrical field, the permanent dipole moment, the electric field, and the exciton polarizability, respectively. The linear and quadratic terms are the contributions from the permanent dipole moment and the electrical-field-induced dipole moment, respectively. The fitting shown in Figure 4d agrees well with the experimental data with $p = -1.63$ D, and $\beta = 3.886 \times 10^{-8}$ Dm/V (1 D = 3.33×10^{-30} C·m). The permanent dipole moment p of the defect states in InSe is comparable to that in a nitrogen-vacancy (NV) defect center (typically between −1.5 to 1.5 D)[40] and monolayer or few-layer MoS_2 (~1.35 D).[41,42] However, the polarizability of the defect state in InSe is almost 6 times larger than that in monolayer MoS_2 (0.58×10^{-8} Dm/V), indicating stronger confinement of the defect state than that in MoS_2. This strong confinement renders the sensitive electrical field dependent on the PL emission, which can be explored for tunable optoelectronic devices. Additional data on the Stark effect can be found in Figure S19.

According to the previous discussion, a fracture has to form to release the large strain of approximately 8.8%.[34,35] We further confirmed that the natural edge of the InSe flake does not give rise to the additional PL peaks, but the edge of a freshly scratched flake showed similar PL spectra as that from the InSe ridge (see the Supporting Information). This suggests that the additional PL might originate from the defects formed due to the mechanical break. To determine a likely defect candidate, we have performed first-principles density functional theory calculations of point defects at the edge of InSe and find that the Se vacancy (V_{Se}) is a prime candidate. The formation energy of the V_{Se} defect along the armchair edge, the structure of which is depicted in Figure 5b, is found to be 0.02

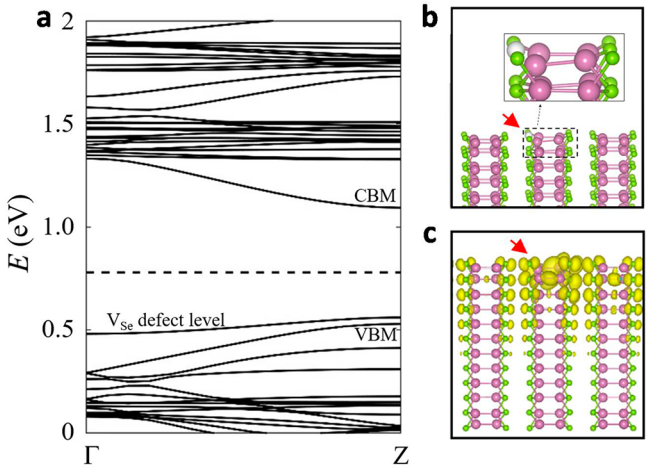

Figure 5. Theoretical calculation of the Se vacancy defect on the InSe armchair edge. (a) Band structure of a defect supercell containing a single Se vacancy on the armchair terminated edge of InSe. The Fermi energy is indicated by the dashed line, and the band associated with the Se defect is shown. (b) Atomic structure of the Se vacancy on the armchair terminated surface of InSe. Red and green spheres represent In and Se atoms, respectively, and the location of the Se vacancy is depicted with a white sphere and indicated by the arrow. (c) An isosurface of the charge density of the defect state associated with the vacancy, indicating that the defect level is spatially localized at the InSe edge in the vicinity of the vacancy.

eV under In-rich conditions, indicating that high concentrations are thermodynamically favorable at room temperature. Furthermore, examination of the band structure associated with this defect, shown in Figure 5a, reveals the presence of a relatively flat occupied shallow acceptor state. An isosurface of the charge density associated with this defect state is depicted in Figure 5c, where it can be seen that the defect state localizes to the vacancy at the edge region. Because this defect level lies above the valence band maximum, it serves as a trap for excitons, wherein the hole associated with an exciton can lower its energy by approximately 30 meV by occupying the V_{Se} defect state. This reduction in exciton energy is consistent with the observed red shift in the PL associated with D-peak, which is observed in the vicinity of the ridge. Furthermore, the V_{Se} trapped exciton model for the observed defect peak would also explain the observed linear Stark effect. As the hole localizes near the edge, it naturally causes anisotropy in the exciton wave function, wherein the electron, which is not as localized as the hole, extends further into the bulk region resulting in a sizable permanent dipole moment. Hence, not only are Se vacancies likely to form at the fracture, but also, their presence would lead to an additional red-shifted excitonic peak at a low temperature that is sensitive to the gate voltage. While the

DOI: 10.1021/acs.nanolett.8b01940
Nano Lett. 2018, 18, 5078−5084

quantitative agreement of the defect exciton binding is most likely fortuitous, the shallow nature of V_{Se} at the edge, combined with its low formation energy, presence of linear Stark effect, and its likelihood to form under mechanical scratch all point toward V_{Se} at the edge as a likely candidate for the origin of the observed D peak.

Conclusions. In summary, we have identified a unique geometric ridge state in 2D InSe flakes. We have exploited the InSe ridge to bypass the selection rule and enhance optical absorption of normally incident light, and we have confirmed this enhancement through PL spectroscopy and scanning photocurrent microscopy. In addition, we observe greatly enhanced light emission from defect states on the ridge, almost 2 orders of magnitude stronger than the intrinsic exciton PL. The emission from the defect states can also be greatly tunable by an external DC gate voltage through the Stark effect thanks to the extremely localized nature of the defect state. The InSe ridge thus provides a new platform for defect engineering which can enable tunable optoelectronic devices in the near-infrared regime.

Experimental Methods. Bulk InSe single crystals were synthesized using the vertical Bridgman method described before,[36] which was used for mechanical exfoliation of InSe flakes with ridges. AFM topographies of the flakes were measured by atomic force microscopy (AFM, Bruker Dimension Icon-PT) operating in tapping mode for the angle and height determination. Mirco-PL measurements were performed at room temperature and low temperatures using a home-built confocal micro-PL spectroscopy setup with the 532 nm laser excitation. PL mapping at room temperature was performed with a Renishaw Invia micro-Raman system with the 532 nm laser excitation. Devices were fabricated by a shadow mask technique followed by e-beam evaporation of 5 nm Ti/100 nm Au electrodes.

SPCM measurements were described previously.[36] A laser beam (a CW or supercontinuum laser) was focused on the samples with a diffraction-limited spot and scanned on the devices mounted on a piezo-stage, while the photocurrent at different positions was recorded by a data acquisition card coupled to a current amplifier. For the excitation-wavelength-dependent photocurrent measurements, a supercontinuum laser (Fianium) with the wavelength ranging from 700 to 1025 nm was used to illuminate the ridge and flat region on the devices.

Our first-principles calculations were based on density functional theory with the Perdew−Burke−Ernzerhof (PBE) approximation to the exchange-correlation function. The interactions between ion cores and valence electrons were described by the projector-augmented wave potentials as implemented in the Vienna ab initio simulation package (VASP). Plane waves with a kinetic energy cutoff of 240 eV were used as the basis set. The calculations were carried out in periodic supercells. The convergence criterion for all atoms is 0.025 eV/Å. A $1 \times 1 \times 2$ k point set was used for the Brillouin zone integration.

■ ASSOCIATED CONTENT

Supporting Information

The Supporting Information is available free of charge on the ACS Publications website at DOI: 10.1021/acs.nanolett.8b01940.

Additional details and figures on angle distribution of ridges, PL and photocurrent enhancement and mapping, and defect emission of InSe flakes. Discussion on origin of the defects, the out-of-plane dipole in 2D InSe, and the Arrhenius equation. (PDF)

■ AUTHOR INFORMATION

Corresponding Authors

*E-mail: shis2@rpi.edu.
*E-mail: zhangs9@rpi.edu.
*E-mail: cy_xu@hit.edu.cn.

ORCID

Raman Sankar: 0000-0003-4702-2517
Rajesh K. Ulaganathan: 0000-0001-8886-6332
Cheng-Yan Xu: 0000-0002-7835-6635
Su-Fei Shi: 0000-0001-5158-805X

Author Contributions

○Y.L., T.W., and H.W. contributed equally.

Notes

The authors declare no competing financial interest.

■ ACKNOWLEDGMENTS

S.-F.S. acknowledges support from the AFOSR under grant no. FA9550-18-1-0312. H.W. and S.B.Z. were supported by the U.S. DOE grant no. DESC0002623. D.W. acknowledges support from the NSF under award no. EFMA-1542798. The supercomputer time was sponsored by NERSC under DOE contract no. DE-AC02-05CH11231, and the CCI at RPI are also acknowledged. The device fabrication was supported by the Micro and Nanofabrication Clean Room (MNCR), operated by the Center for Materials, Devices, and Integrated Systems (cMDIS) at Rensselaer Polytechnic Institute (RPI). C.-Y.X. acknowledges support from National Natural Science Foundation of China (no. 51572057).

■ REFERENCES

(1) Wang, Q. H.; Kalantar-Zadeh, K.; Kis, A.; Coleman, J. N.; Strano, M. S. Electronics and optoelectronics of two-dimensional transition metal dichalcogenides. *Nat. Nanotechnol.* **2012**, *7*, 699−712.

(2) Chhowalla, M.; Jena, D.; Zhang, H. Two-dimensional semiconductors for transistors. *Nature Reviews Materials* **2016**, *1*, 16052.

(3) Mak, K. F.; Shan, J. Photonics and optoelectronics of 2D semiconductor transition metal dichalcogenides. *Nat. Photonics* **2016**, *10*, 216−226.

(4) Mak, K. F.; Lee, C.; Hone, J.; Shan, J.; Heinz, T. F. Atomically Thin MoS_2: A New Direct-Gap Semiconductor. *Phys. Rev. Lett.* **2010**, *105*, 136805.

(5) Splendiani, A.; Sun, L.; Zhang, Y.; Li, T.; Kim, J.; Chim, C. Y.; Galli, G.; Wang, F. Emerging photoluminescence in monolayer MoS_2. *Nano Lett.* **2010**, *10*, 1271−1275.

(6) Mak, K. F.; He, K.; Shan, J.; Heinz, T. F. Control of valley polarization in monolayer MoS_2 by optical helicity. *Nat. Nanotechnol.* **2012**, *7*, 494−498.

(7) Xiao, D.; Liu, G. B.; Feng, W.; Xu, X.; Yao, W. Coupled spin and valley physics in monolayers of MoS_2 and other group-VI dichalcogenides. *Phys. Rev. Lett.* **2012**, *108*, 196802.

(8) Schaibley, J. R.; Yu, H. Y.; Clark, G.; Rivera, P.; Ross, J. S.; Seyler, K. L.; Yao, W.; Xu, X. D. Valleytronics in 2D materials. *Nature Reviews Materials* **2016**, *1*, 16055.

(9) Radisavljevic, B.; Radenovic, A.; Brivio, J.; Giacometti, V.; Kis, A. Single-layer MoS_2 transistors. *Nat. Nanotechnol.* **2011**, *6*, 147−150.

(10) Bao, W. Z.; Cai, X. H.; Kim, D.; Sridhara, K.; Fuhrer, M. S. High mobility ambipolar MoS_2 field-effect transistors: Substrate and dielectric effects. *Appl. Phys. Lett.* **2013**, *102*, 042104.

DOI: 10.1021/acs.nanolett.8b01940
Nano Lett. 2018, 18, 5078−5084

(11) Bernardi, M.; Palummo, M.; Grossman, J. C. Extraordinary sunlight absorption and one nanometer thick photovoltaics using two-dimensional monolayer materials. *Nano Lett.* **2013**, *13*, 3664−3670.
(12) Jariwala, D.; Davoyan, A. R.; Tagliabue, G.; Sherrott, M. C.; Wong, J.; Atwater, H. A. Near-Unity Absorption in van der Waals Semiconductors for Ultrathin Optoelectronics. *Nano Lett.* **2016**, *16*, 5482−5487.
(13) Mudd, G. W.; Svatek, S. A.; Ren, T.; Patanè, A.; Makarovsky, O.; Eaves, L.; Beton, P. H.; Kovalyuk, Z. D.; Lashkarev, G. V.; Kudrynskyi, Z. R.; et al. Tuning the bandgap of exfoliated InSe nanosheets by quantum confinement. *Adv. Mater.* **2013**, *25*, 5714−5718.
(14) Bandurin, D. A.; Tyurnina, A. V.; Geliang, L. Y.; Mishchenko, A.; Zólyomi, V.; Morozov, S. V.; Kumar, R. K.; Gorbachev, R. V.; Kudrynskyi, Z. R.; Pezzini, S.; et al. High electron mobility, quantum Hall effect and anomalous optical response in atomically thin InSe. *Nat. Nanotechnol.* **2017**, *12*, 223.
(15) Sánchez-Royo, J. F.; Muñoz-Matutano, G.; Brotons-Gisbert, M.; Martínez-Pastor, J. P.; Segura, A.; Cantarero, A.; Mata, R.; Canet-Ferrer, J.; Tobias, G.; Canadell, E.; et al. Electronic structure, optical properties, and lattice dynamics in atomically thin indium selenide flakes. *Nano Res.* **2014**, *7*, 1556−1568.
(16) Sucharitakul, S.; Goble, N. J.; Kumar, U. R.; Sankar, R.; Bogorad, Z. A.; Chou, F. C.; Chen, Y. T.; Gao, X. P. Intrinsic Electron Mobility Exceeding 10^3 $cm^2/(V\ s)$ in Multilayer InSe FETs. *Nano Lett.* **2015**, *15*, 3815−3819.
(17) Mudd, G. W.; Molas, M. R.; Chen, X.; Zolyomi, V.; Nogajewski, K.; Kudrynskyi, Z. R.; Kovalyuk, Z. D.; Yusa, G.; Makarovsky, O.; Eaves, L.; et al. The direct-to-indirect band gap crossover in two-dimensional van der Waals Indium Selenide crystals. *Sci. Rep.* **2016**, *6*, 39619.
(18) Tamalampudi, S. R.; Lu, Y.-Y.; Kumar U, R.; Sankar, R.; Liao, C.-D.; Moorthy B, K.; Cheng, C.-H.; Chou, F. C.; Chen, Y.-T. High performance and bendable few-layered InSe photodetectors with broad spectral response. *Nano Lett.* **2014**, *14*, 2800−2806.
(19) Lei, S.; Ge, L.; Najmaei, S.; George, A.; Kappera, R.; Lou, J.; Chhowalla, M.; Yamaguchi, H.; Gupta, G.; Vajtai, R.; et al. Evolution of the electronic band structure and efficient photo-detection in atomic layers of InSe. *ACS Nano* **2014**, *8*, 1263−1272.
(20) Luo, W. G.; Cao, Y. F.; Hu, P. G.; Cai, K. M.; Feng, Q.; Yan, F. G.; Yan, T. F.; Zhang, X. H.; Wang, K. Y. Gate Tuning of High-Performance InSe-Based Photodetectors Using Graphene Electrodes. *Adv. Opt. Mater.* **2015**, *3*, 1418−1423.
(21) Do, D. T.; Mahanti, S. D.; Lai, C. W. Spin splitting in 2D monochalcogenide semiconductors. *Sci. Rep.* **2015**, *5*, 17044.
(22) Liang, W. Y. Optical anisotropy in layer compounds. *J. Phys. C: Solid State Phys.* **1973**, *6*, 551.
(23) Liang, W. Y. Optical anisotropy in GaSe. *J. Phys. C: Solid State Phys.* **1975**, *8*, 1763.
(24) Brotons-Gisbert, M.; Andres-Penares, D.; Suh, J.; Hidalgo, F.; Abargues, R.; Rodriguez-Canto, P. J.; Segura, A.; Cros, A.; Tobias, G.; Canadell, E.; Ordejon, P.; Wu, J.; Martinez-Pastor, J. P.; Sanchez-Royo, J. F. Nanotexturing To Enhance Photoluminescent Response of Atomically Thin Indium Selenide with Highly Tunable Band Gap. *Nano Lett.* **2016**, *16*, 3221−3229.
(25) Tang, Y. H.; Xie, W.; Mandal, K. C.; McGuire, J. A.; Lai, C. W. Linearly Polarized Remote-Edge Luminescence in GaSe Nanoslabs. *Phys. Rev. Appl.* **2015**, *4*, 034008.
(26) Leavitt, R. P.; Bradshaw, J. L.; Pham, J. T.; Tobin, M. S. Quantitative Model for Photocurrent Spectroscopy of Quantum-Well Diodes Including Transit-Time and Background-Doping Effects. *J. Appl. Phys.* **1994**, *75*, 2215−2226.
(27) Hyun, J. K.; Lauhon, L. J. Spatially Resolved Plasmonically Enhanced Photocurrent from Au Nanoparticles on a Si Nanowire. *Nano Lett.* **2011**, *11*, 2731−2734.
(28) Brittman, S.; Gao, H. W.; Garnett, E. C.; Yang, P. D. Absorption of Light in a Single-Nanowire Silicon Solar Cell Decorated with an Octahedral Silver Nanocrystal. *Nano Lett.* **2011**, *11*, 5189−5195.
(29) Varshni, Y. P. Temperature dependence of the energy gap in semiconductors. *Physica* **1967**, *34*, 149.
(30) Goni, A. R.; Cantarero, A.; Chevy, A.; Schwarz, U.; Syassen, K. Low-Temperature Exciton Absorption in InSe under Pressure. *Phys. Rev. B: Condens. Matter Mater. Phys.* **1992**, *45*, 4221−4226.
(31) Kuroda, N.; Munakata, I.; Nishina, Y. Exciton transitions from spin-orbit split off valence bands in layer compound InSe. *Solid State Commun.* **1980**, *33*, 687−691.
(32) Cingolani, A.; Cingolani, R.; Ferrara, M.; Lugara, M. The resonant nature of the direct exciton in InSe. *Solid State Commun.* **1986**, *57*, 63−65.
(33) Imai, K. Excitonic photoluminescence properties of InSe. *J. Lumin.* **1989**, *43*, 121−124.
(34) Castellanos-Gomez, A.; Roldan, R.; Cappelluti, E.; Buscema, M.; Guinea, F.; van der Zant, H. S.; Steele, G. A. Local strain engineering in atomically thin MoS_2. *Nano Lett.* **2013**, *13*, 5361−5366.
(35) Mosca, D. H.; Mattoso, N.; Lepienski, C. M.; Veiga, W.; Mazzaro, I.; Etgens, V. H.; Eddrief, M. Mechanical properties of layered InSe and GaSe single crystals. *J. Appl. Phys.* **2002**, *91*, 140−144.
(36) Li, Y.; Wang, T.; Wu, M.; Cao, T.; Chen, Y.; Sankar, R.; Ulaganathan, R. K.; Chou, F.-C.; Wetzel, C.; Xu, C.; et al. Ultrasensitive tunability of the direct bandgap of two-dimensional InSe flakes via strain engineering. *2D Mater.* **2018**, *5*, 021002.
(37) Empedocles, S. A.; Bawendi, M. G. Quantum-confined stark effect in single CdSe nanocrystallite quantum dots. *Science* **1997**, *278*, 2114−2117.
(38) Hache, F.; Ricard, D.; Flytzanis, C. Quantum-Confined Stark-Effect in Very Small Semiconductor Crystallites. *Appl. Phys. Lett.* **1989**, *55*, 1504−1506.
(39) Wen, G. W.; Lin, J. Y.; Jiang, H. X.; Chen, Z. Quantum-Confined Stark Effects in Semiconductor Quantum Dots. *Phys. Rev. B: Condens. Matter Mater. Phys.* **1995**, *52*, 5913−5922.
(40) Tamarat, P.; Gaebel, T.; Rabeau, J. R.; Khan, M.; Greentree, A. D.; Wilson, H.; Hollenberg, L. C. L.; Prawer, S.; Hemmer, P.; Jelezko, F.; Wrachtrup, J. Stark shift control of single optical centers in diamond. *Phys. Rev. Lett.* **2006**, *97*, 083002.
(41) Klein, J.; Wierzbowski, J.; Regler, A.; Becker, J.; Heimbach, F.; Muller, K.; Kaniber, M.; Finley, J. J. Stark Effect Spectroscopy of Mono- and Few-Layer MoS_2. *Nano Lett.* **2016**, *16*, 1554−1559.
(42) Roch, J. G.; Leisgang, N.; Froehlicher, G.; Makk, P.; Watanabe, K.; Taniguchi, T.; Schönenberger, C.; Warburton, R. J. Quantum-Confined Stark Effect in a MoS_2 Monolayer van der Waals Heterostructure. *Nano Lett.* **2018**, *18*, 1070−1074.
(43) Mak, K. F.; He, K.; Lee, C.; Lee, G. H.; Hone, J.; Heinz, T. F.; Shan, J. Tightly bound trions in monolayer MoS_2. *Nat. Mater.* **2013**, *12*, 207−211.
(44) Ross, J. S.; Wu, S.; Yu, H.; Ghimire, N. J.; Jones, A. M.; Aivazian, G.; Yan, J.; Mandrus, D. G.; Xiao, D.; Yao, W.; Xu, X. Electrical control of neutral and charged excitons in a monolayer semiconductor. *Nat. Commun.* **2013**, *4*, 1474.

DOI: 10.1021/acs.nanolett.8b01940
Nano Lett. 2018, 18, 5078−5084